Alignment-dependent ionization of H_2^+: From multiphoton ionization to tunneling ionization

Bin Zhang, Jianmin Yuan, and Zengxiu Zhao*

Department of Physics, National University of Defense Technology, ChangSha, 410073, P. R. China

(Received 14 January 2012; published 19 March 2012)

We investigate the strong-field ionization for the ground state of H_2^+ by numerically solving the three-dimensional (3D) time-dependent Schrödinger equation (TDSE), and comparisons have been made among the TDSE, the different versions of molecular strong-field approximation (MO-SFA) and the molecular Ammosov-Delone-Krainov (MO-ADK) approximation. The study shows that, for the TDSE results, the ratio of ionization rates between perpendicular and parallel alignments displays a step-like structure against the Keldysh parameter γ. For small internuclear distances, the transition between the steps are found to be around $\gamma \approx 1$ and is recognized as the competition between the multiphoton ionization (MPI) and tunneling ionization (TI). The ionization is more isotropic in the MPI regime. For large internuclear distances, the transition position shifts to larger γ due to the charge-resonance-enhanced ionization (CREI). Different versions of strong-field ionization theories are compared against the TDSE results.

DOI: 10.1103/PhysRevA.85.033421 PACS number(s): 32.80.Rm, 42.50.Hz, 42.65.Ky

I. INTRODUCTION

Strong-field ionization is a fundamental atomic and molecular process in strong laser fields that has continued to attract much attention in the recent past, both experimentally and theoretically [1–3], especially because the recent advances in laser technology have made possible experimental investigation of molecular processes on an ultrashort time scale and under ultrastrong laser intensity [4–6]. Due to the extra degrees of freedom, the response of molecules to strong fields is considerably more complicated than that of atoms, which poses great theoretical and computational challenge. Diatomic molecules are of fundamental importance in this regard and provide an important test bed. For diatomic molecules, the extra degrees of freedom are the internuclear separation R, and the orientation of the molecular axis with respect to the laser field polarization, which can be controlled by pulsed lasers [7]. This paper is focused on the accurate treatment of the dependance of strong-field ionization on the orientation effects.

Great difficulty still exists even for the theoretical investigations of multielectron diatomic molecules. Approximate models are widely used, such as the molecular Ammosov-Delone-Krainov (MO-ADK) approximation [8,9] and the molecular strong-field approximation (MO-SFA)[or referenced as the Keldysh-Faisal-Reiss (KFR) approximation] [10–12]. However, problems may arise in the actual calculations. The MO-ADK approximation is a tunneling theory and is only valid in the tunneling regime when the optical period is much less than the characteristic time of tunneling [10].

For the MO-SFA, two gauges are commonly used for the description of strong-field ionization: the length gauge (LG) and the velocity gauge (VG). Partly due to the perturbative nature of the SFA, the should-be gauge invariance of physical observables obtained from the LG and the VG differ and the two gauges turn out to be two distinct approximations, giving qualitatively conflicting results in many studies [13–15]. On the other hand, the simplest diatomic molecule H_2^+ is a unique one-electron molecular system which allows for almost exact solutions in the field-free case, as well as for accurate treatment in a laser field, with the recently developed nonperturbative methods of solving the three-dimensional (3D) time-dependent Schrödinger equation (TDSE) [16–18]. It can be used to benchmark these basic theoretical models. The electron orbitals with the same symmetry exist in stable multielectron systems, which have recently been a subject of extensive experimental [19–21] and theoretical explorations. The finding that the alignment dependence of ionization rates varies with laser intensity in this work may provide useful insights for the understanding of multielectron effects in more complex molecules, such as strong-field ionization and high-harmonic generation (HHG) from multiple orbitals [22–24].

The organization of this paper is as follows: In Sec. II we briefly describe the numerical method of solving the 3D TDSE and the theoretical models MO-ADK and MO-SFA. Section III gives the calculation details. In Sec. IV, we present our results regarding the strong-field ionization from the ground state of H_2^+. The TDSE results are compared with those from the MO-ADK and MO-SFA models and detailed discussions are presented. We conclude in Sec. V.

II. THEORY

A. TDSE

If the molecular axis of the diatomic molecular ion H_2^+ is directed along the z axis and the nuclei are located on this axis at the positions $-a$ and a (so the internuclear separation $R = 2a$), then the prolate spheroidal coordinates ξ, η, and φ which are related to the Cartesian coordinates x, y, and z are as follows [25]:

$$\begin{aligned} x &= a\sqrt{(\xi^2-1)(1-\eta^2)}\cos\varphi, \\ y &= a\sqrt{(\xi^2-1)(1-\eta^2)}\sin\varphi, \quad z = a\xi\eta. \end{aligned} \tag{1}$$

*zhao.zengxiu@gmail.com

We obtain the ground-state wave function by solving the unperturbed eigenvalue problem, which reads

$$\left[-\tfrac{1}{2}\nabla^2 + V(\xi,\eta)\right]\Psi(\xi,\eta,\varphi) = E\Psi(\xi,\eta,\varphi). \tag{2}$$

Here the Laplacian operator in the prolate spheroidal coordinates is

$$\nabla^2 = \frac{1}{a^2(\xi^2-\eta^2)}\left[\frac{\partial}{\partial\xi}(\xi^2-1)\frac{\partial}{\partial\xi} + \frac{\partial}{\partial\eta}(1-\eta^2)\frac{\partial}{\partial\eta} + \frac{\xi^2-\eta^2}{(\xi^2-1)(1-\eta^2)}\frac{\partial^2}{\partial\varphi^2}\right], \tag{3}$$

and the Coulomb interaction with the nuclei is as follows (the charge of each center is unity for $H_2{}^+$):

$$V(\xi,\eta) = -\frac{2\xi}{a(\xi^2-\eta^2)}. \tag{4}$$

If the wave function $\Psi(\xi,\eta,\varphi)$ is expanded in a Fourier series with respect to the angular coordinate,

$$\Psi(\xi,\eta,\varphi) = \sum_m \psi_m(\xi,\eta)\exp(im\varphi), \tag{5}$$

we get the separated eigenvalue problems for $|m|$,

$$E\psi_m = -\frac{1}{2a^2(\xi^2-\eta^2)}\left[\frac{\partial}{\partial\xi}(\xi^2-1)\frac{\partial}{\partial\xi} + \frac{\partial}{\partial\eta}(1-\eta^2)\frac{\partial}{\partial\eta} - \frac{m^2(\xi^2-\eta^2)}{(\xi^2-1)(1-\eta^2)} + 4a\xi\right]\psi_m. \tag{6}$$

Equation (6) is solved by expanding the wave function $\psi_m(\xi,\eta)$ in a product basis of discrete-variable-representation (DVR) functions,

$$\psi_m(\xi,\eta) = \sum_{i,j} c_{ij}^m \chi_i^\xi(\xi)\chi_j^\eta(\eta). \tag{7}$$

Note that the exact eigenfunctions have factors $(\xi^2-1)^{|m|/2}(1-\eta^2)^{|m|/2}$ which are nonanalytical at nuclei for odd m [26]. Measures have to be done to ensure accurate numerical solutions of the differential equations for both even and odd projections of angular momentum. For the even m, the DVR functions are [18]

$$\chi_n^\xi(\xi) = \frac{1}{\sqrt{w_n^\xi}}\prod_{i\neq n}^{N_\xi}\frac{\xi-\xi_i}{\xi_n-\xi_i}, \quad \chi_n^\eta(\eta) = \frac{1}{\sqrt{w_n^\eta}}\prod_{i\neq n}^{N_\eta}\frac{\eta-\eta_i}{\eta_n-\eta_i}, \tag{8}$$

while for the odd m, the DVR functions are defined as

$$\chi_n^\xi(\xi) = \frac{1}{\sqrt{w_n^\xi}}\sqrt{\frac{\xi^2-1}{\xi_n^2-1}}\prod_{i\neq n}^{N_\xi}\frac{\xi-\xi_i}{\xi_n-\xi_i}, \qquad \chi_n^\eta(\eta) = \frac{1}{\sqrt{w_n^\eta}}\sqrt{\frac{1-\eta^2}{1-\eta_n^2}}\prod_{i\neq n}^{N_\eta}\frac{\eta-\eta_i}{\eta_n-\eta_i}, \tag{9}$$

where $(\xi_i, w_i^\xi)/(\eta_i, w_i^\eta)$ are the points and associated weights corresponding to some specified N^ξ/N^η-point Gauss quadrature [25]. The variable ξ, which runs from 1 to some specified maximum value $\xi_{\max}$, is mapped to the interval $[-1,1]$, and then discretized using the Gauss-Radau quadrature. On the other hand, the Gauss-Legendre quadrature is used for the variable η.

The time-dependent Schrödinger equation in the laser field is solved by means of the split-operator method. We employ the following second-order propagation operator [27]:

$$\Psi(t+\Delta t) = \exp\left(-i\frac{\Delta t}{2}H_0\right)\exp\left[-i\Delta t U\left(t+\frac{\Delta t}{2}\right)\right] \times \exp\left(-i\frac{\Delta t}{2}H_0\right)\Psi(t) + O[(\Delta t)^3]. \tag{10}$$

Here Δt is the time propagation step, H_0 is the unperturbed electronic Hamiltonian which includes the kinetic energy and the interaction with the nuclei, and $U(t)$ is the term due to the coupling to the external field. In the length gauge, for a linearly polarized (in the x-z plane) laser field, the potential U reads

$$U(\xi,\eta,\varphi,t) = aF(t)[\sqrt{(\xi^2-1)(1-\eta^2)}\cos\varphi\sin\theta + \xi\eta\cos\theta]. \tag{11}$$

Here θ is the angle between the polarization vector of the laser field and the molecular axis. $F(t)$ is the electric field.

The field-free propagator $\exp(-i\frac{1}{2}\Delta t H_0)$ needs only be constructed once before the propagation, using the energy values and eigenstates of the unperturbed system. The external field operator $\exp(-i\Delta t V)$ is diagonal in coordinate representation when using the length gauge. For efficient matrix and vector operations we use the basic linear algebra subroutines (BLAS) [28] and the linear algebra package (LAPACK) [29].

B. MO-ADK

The molecular ADK (MO-ADK) theory is a generalization of the atomic ADK theory [31]. The requirement for the validity of the tunneling model for an oscillating field is that the width of the barrier does not change during the time the electron spends traversing it; that is, the electron adiabatically follows the change in the external field. Whether this assumption is reasonable or not depends on the value of the Keldysh parameter [10]

$$\gamma = \sqrt{2I_p}(\omega/F), \tag{12}$$

with $\gamma \ll 1$ in the tunneling regime. Here I_p is the ionization potential. F and ω are the field strength and frequency, respectively, of the external field.

The cycle-averaged ionization rate reads [9]

$$W = \sqrt{\frac{3F_0}{\pi\kappa^3}}\frac{W_{\text{stat}}^+ + W_{\text{stat}}^-}{2}, \tag{13}$$

where the static rates for the positive and negative field directions are

$$W_{\text{stat}}^\pm(F,\mathbf{R}) = \sum_{m'}\frac{|B^\pm(m')|^2 e^{\frac{-2k^3}{3F}}}{2^{m'}|m'|!k^{\frac{2Z_c}{k}-1}}\left(\frac{2k^3}{F}\right)^{\frac{2Z_c}{k}-|m'|-1}, \tag{14}$$

with

$$B^{\pm}(m') = \sum_{l,m} (-1)^{\frac{|m'|+m'}{2}} \sqrt{\frac{(2l+1)(l+|m'|)!}{2(l-|m'|)!}} C^{\pm}_{lm} D^{l}_{m'm}(\mathbf{R}), \tag{15}$$

and $C^{+}_{lm} = C_{lm}$, $C^{-}_{lm} = (-1)^l C_{lm}$. In fact, for parity eigenstates, corresponding to inversion-symmetric molecules, $W^{+}_{\rm stat}(F,\mathbf{R}) = W^{-}_{\rm stat}(F,\mathbf{R})$ [32]. $D^{l}_{m'm}(\phi,\theta,\chi)$ is the Wigner rotation function [33], where $\mathbf{R} = (\phi,\theta,\chi)$ is the Euler angle between the molecule-fixed frame and the space-fixed frame. Z_c is the charge of the residual ion and $k = \sqrt{2I_p}$. The asymptotic coefficients C_{lm} can be determined by matching the radial partial wave function $F_{lm}(r)$ [$= \int d\mathbf{\Omega} Y^{*}_{lm}(\theta,\phi)\Phi_0(\mathbf{r})$] to the form $C_{lm} r^{(Z_c/k)-1} e^{-kr}$ in the asymptotic region.

C. MO-SFA

For a linearly polarized electric field $\mathbf{F}(t) = \mathbf{F}_0 \sin(\omega t)$ with associated vector potential $\mathbf{A}(t) = \mathbf{A}_0 \cos(\omega t)(A_0 = F_0/\omega)$, the total ionization rate $W = \int d\mathbf{\Omega}_{\mathbf{p}} dW/d\mathbf{\Omega}_{\mathbf{p}}$, where the angular differential ionization rate $dW/d\mathbf{\Omega}_{\mathbf{p}}$ can be written as the sum over n-photon processes [34]

$$\frac{dW}{d\mathbf{\Omega}_{\mathbf{p}}} = 2\pi N_e \sum_{n=n_0}^{\infty} |A_n|^2 p_n, \tag{16}$$

where the momentum $p_n = \sqrt{2(nw - I_p - U_p)}$, with I_p being the binding energy of the initially bound electron and $U_p = F_0^2/(4w^2)$ being the ponderomotive potential. Energy conservation determines the minimum number of photons needed to reach the continuum, $n_0 = \lceil (I_p + U_p)/w \rceil$. The transition amplitudes A_n is

$$A^{c}_{n} = \frac{1}{T} \int_0^T dt e^{iS(t)} D^{c}_{n}(t), \tag{17}$$

where

$$D^{c}_{n}(t) = \begin{cases} \langle \mathbf{q}(t)|\mathbf{F}(t)\cdot\mathbf{r}|0\rangle & (c = LG) \\ \langle \mathbf{p}_n|[\mathbf{A}(t)\cdot\mathbf{p}_n + \mathbf{A}^2(t)/2]|0\rangle & (c = VG), \end{cases} \tag{18}$$

with the time-dependent momentum $\mathbf{q}(t) = \mathbf{p}_n + \mathbf{A}(t)$ and $S(t) = \int^t dt_0[\mathbf{q}^2(t_0)/2 + I_p]$. $|0\rangle$ is the ground-state wave function. $|\mathbf{p}_n\rangle = (2\pi)^{-3/2}\exp(i\mathbf{p}_n\cdot\mathbf{r})$. Equation (17) contains a fast-oscillating term $\exp[iS(t)]$ and is integrated using the saddle-point approximation, yielding [35]

$$A^{c}_{n} = \frac{1}{T} \sum_{s} \sqrt{\frac{2\pi i}{\mathbf{F}(t_s)\cdot\mathbf{q}(t_s)}} e^{iS(t_s)} D^{c}_{n}(t_s), \tag{19}$$

where the summation is over the two saddle points $t = t_s$ with $0 < \mathrm{Re}t_s < T$ and $\mathrm{Im}t_s > 0$ that are solutions of the equation

$$\partial S(t)/\partial t = I_p + [\mathbf{p} + \mathbf{A}(t)]^2/2 = 0. \tag{20}$$

Let $\mathbf{A} = \hat{\mathbf{e}}_A A = \hat{\mathbf{e}}_A(A_r + iA_i)$, where $\hat{\mathbf{e}}_A$ is the unit vector in the direction of $\mathbf{A}$, and A_r and A_i denote the real and imaginary parts of A, respectively. The real and imaginary parts of the saddle-point equation are

$$A_i(A_r + p_{\parallel}) = 0, \quad p_{\perp}^2 - A_i^2 + 2I_p = 0, \tag{21}$$

where $p_{\perp}$ and $p_{\parallel}$ are the component of $\mathbf{p}$ parallel and perpendicular to the vector potential $\mathbf{A}$, respectively. The solutions are $\mathbf{A}(t_s) = \hat{e}_A[-p_{\parallel} \pm i(2I_p + p_{\perp}^2)^{1/2}]$.

TABLE I. Energies of the ground state ($1\sigma_g$) of H_2^+ at different internuclear separations. The reference data are taken from Ref. [30].

R(a.u.)	Energy (a.u.)	Reference energy (a.u.)
1	− 1.451 786 313 378 435	− 1.451 786 313 3781
2	− 1.102 634 214 494 976	− 1.102 634 214 4949
3	− 0.910 896 197 382 3676	− 0.910 896 197 3823
4	− 0.796 084 883 712 9860	− 0.796 084 883 7129
6	− 0.678 635 715 133 3285	− 0.678 635 715 1334
8	− 0.627 570 388 599 9898	− 0.627 570 388 6000

III. CALCULATION

The numerical parameters of the present calculations are as follows: The ξ grid runs from 1 to the maximum value $\xi_{\rm max}$ at which the grid is truncated. In this paper, we set $\xi_{\rm max} = R_{\rm max}/a$, so that the size of the simulation box can be kept fixed at $\max(R) = \max(a\sqrt{\xi^2+\eta^2-1}) = R_{\rm max}$. We use 120 DVR functions in ξ and 18 DVR functions in η. The angular momentum projections are kept from $m = -8$ to $m = 8$. Convergence is achieved with the above settings. Table I gives the energies of the ground state ($1\sigma_g$) of H_2^+ at different internuclear separations. All digits are accurate and the results are obtained with machine accuracy.

For the time propagation, we use 4096 time steps per optical cycle and an absorbing layer between $R_b = 40$ and $R_{\rm max} = 80$ is used to smoothly brings down the wave function and prevents an unphysical reflection from the boundary. In this paper, the electric field $F(t)$ is chosen as a 20-optical sine-squared-shape pulse, $F(t) = F_0 \sin^2(\pi t/T)\sin(\omega t)$, where F_0 is the peak field amplitude, ω is the laser frequency, and T is the pulse duration. After the time propagation, the ionization rate W is then obtained by fitting the norm to the formula $|\Psi(t)|^2 = \exp[-W(t-t_0)]|\Psi(t_0)|^2$. Ionization saturation is avoided in all calculations.

The field-free eigenstate wave function is used as the input to calculate the MO-ADK asymptotic coefficients C_{lm}. In Fig. 1 we show the radial partial wave $F_{lm}(r)$ for the $1\sigma_g$ state of H_2^+ ($R = 2$ a.u.), using the wave function calculated by TDSE and GAMESS [36]. For the GAMESS calculation, we have used the augmented correlation-consistent polarized triple-zeta (aug-cc-pVTZ) basis set [37]. Due to the symmetries of the $1\sigma_g$ state, only the partial waves with $L =$ even and $m = 0$ exist. It is obvious that the GAMESS wave function fails to correctly describe the asymptotic behavior in the long-range Coulomb potential, which leads to numerical uncertainties and even erroneous results in the calculation of asymptotic coefficients. On the other hand, the values for F_{lm} extracted from the TDSE wave function display correct asymptotic behavior, even with large quantum number L. Table II gives the asymptotic coefficients for the $1\sigma_g$ state of H_2^+ at different internuclear separations. As expected, the ratio C_{20}/C_{00}, which reflects the nonspherical symmetry of the electronic density distribution, increases with the internuclear distance. For the

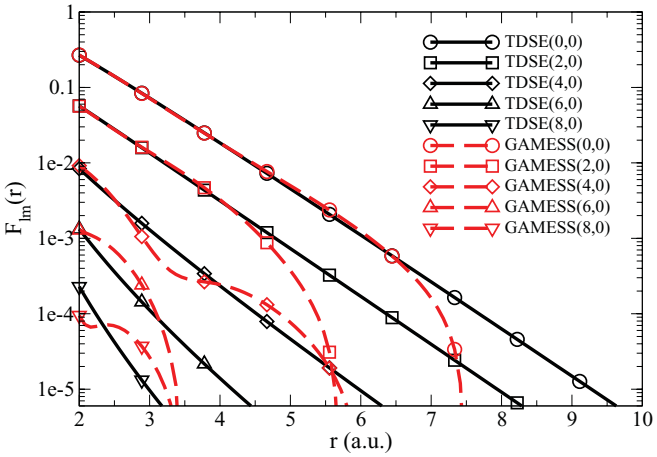

FIG. 1. (Color online) Radial partial wave $F_{lm}(r)$ for the $1\sigma_g$ state of H_2^+, using the wave function calculated by TDSE (solid lines) and GAMESS (dashed lines). The angular momentum numbers L are 0 (○-○), 2 (□-□), 4 (◇-◇), 6 (△-△), and 8 (▽-▽).

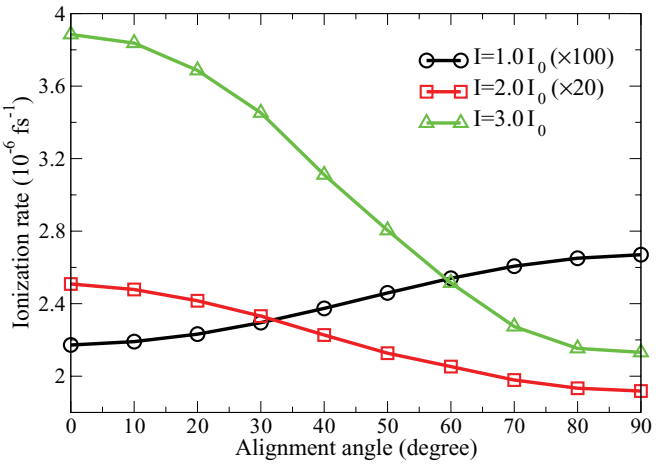

FIG. 2. (Color online) Normalized (to the maximum) ionization rates versus alignment angle θ when the internuclear distance $R = 2$ a.u. for the $1\sigma_g$ state of H_2^+. The laser intensities are $1.0I_0$ (○-○,×100), $2.0I_0$ (□-□,×20), and $3.0I_0$ (△-△), respectively. The laser carrier wavelength is 800 nm.

LG-SFA and VG-SFA, the ground-state wave functions are directly inserted into Eq. (18) to calculate the ionization rates.

IV. RESULTS AND DISCUSSION

A. Numerical results

In this paper, we will use $I_0 = 1 \times 10^{14}$ W/cm^2 as the unit of laser intensity since we are interested in the laser intensity in the order of I_0. In Fig. 2, we present the ionization rates as functions of the alignment angle between the laser polarization direction and the molecular axis, for the following peak intensities of the laser field: $1.0I_0$, $2.0I_0$, and $3.0I_0$, for the $1\sigma_g$ state. The internuclear distance $R = 2$ a.u. The carrier frequency $\omega = 0.056\,95$ a.u., corresponding to the wavelength 800 nm. For the intensity $3.0I_0$, the ionization rate decreases monotonically with θ increasing from 0° to 90°. The ratio $W(90°)/W(0°)$ is 0.55, in good agreement with the result of Ref. [17] (≈0.59). For the intensity $2.0I_0$, the ionization rate has a similar behavior, except that the ratio $W(90°)/W(0°)$ changes to 0.81. For these two intensities, the parallel aligned molecules are easier to ionize as compared to the perpendicular case. However, the situation changes for the lower intensity $1.0I_0$. The ionization rate increases monotonically with θ increasing from 0° to 90°, resulting in a ratio of 1.2. At this intensity, the perpendicularly aligned molecules become easier to ionize, in qualitative disagreement with the higher-intensities ($2.0I_0$ and $3.0I_0$) cases. On the other hand, as far as the ratio $W(90°)/W(0°)$ is considered, it is in inverse proportion to the laser peak intensity. The same can be observed in the calculations of Ref. [16,17]. The ratio $W(90°)/W(0°)$ depends critically on the laser peak intensity.

TABLE II. Asymptotic coefficients (C_{lm}) for the $1\sigma_g$ state of H_2^+ at different internuclear separations, as obtained from the present calculations and from the literature.

R(a.u.)	C_{00}	C_{20}	C_{40}	C_{60}	C_{80}
1	6.480	0.398	0.024		
2	4.464	0.589	0.023		
2[a]	4.37	0.05			
3	4.092	1.045	0.076		
4	3.957	1.608	0.183	0.012	
6	4.438	3.314	0.708	0.086	
8	6.178	6.504	2.118	0.401	0.054

[a]Reference [8].

Strong-field ionization can be qualitatively classified by the so-called Keldysh parameter γ [see Eq. (12)] [10]. When $\gamma > 1$, corresponding to the low-laser-intensity case, the ionization is dominated by the multiphoton ionization channel. However, as the laser intensity increases, tunneling ionization channel starts to play a role or even dominates the total ionization ($\gamma < 1$). For the parameters used in Fig. 2 ($I_p = 1.1026$ a.u., $\omega = 0.05695$ a.u.), the γ values for the intensities $1.0I_0$, $2.0I_0$, and $3.0I_0$ are 1.2, 0.8, and 0.5, respectively. The intensity $1.0I_0$ corresponds to the multiphoton ionization region, while the intensity $3.0I_0$ lies in the tunneling ionization region. The ratio $W(90°)/W(0°)$ varies as the competition between MPI and TI.

The above argument is further investigated in Fig. 3. In Fig. 3, the ratios of ionization rate $[W(90°)/W(0°)]$ are presented as functions of the Keldysh parameter for the $1\sigma_g$ state, where the laser wavelength is fixed at 800 nm and the internuclear distance takes the following values: 1 a.u., 2 a.u., 3 a.u., 4 a.u., 6 a.u., and 8 a.u., respectively. For all these internuclear distances, the ratios display an obvious two-step-like behavior: one step at each of the two γ-axis limits with a transition at some critical values. For the small distances ($R = 1$ a.u., 2 a.u., and 3 a.u.), the transitions take place approximately at a critical value of $\gamma \approx 1$. The ratio of the lower steps are 0.8, 0.6, and 0.4, respectively, reflecting the asymmetry of electronic density distribution with increasing the internuclear distance, as expected. Exceptions occur with larger distances ($R = 4$ a.u., 6 a.u., and 8 a.u.), where the transition points deviate from $\gamma = 1$ (≈4) and the lower step ratios suddenly drop to nearly 0. We attribute this to the

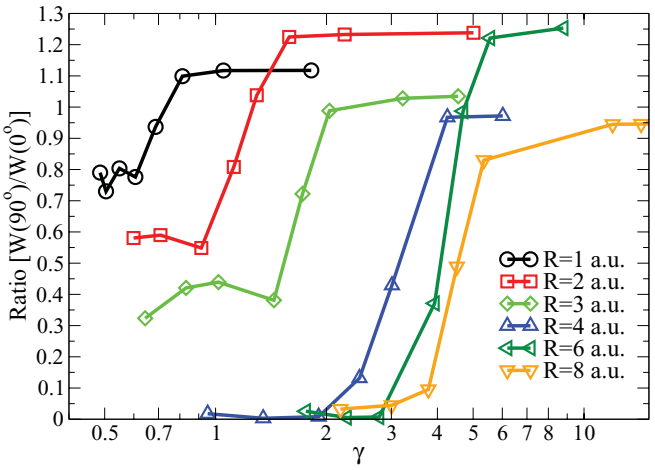

FIG. 3. (Color online) Ratios of ionization rate $[W(90°)/W(0°)]$ versus the Keldysh parameter for the $1\sigma_g$ state of H_2^+. The internuclear separations are 1 a.u. (○-○), 2 a.u. (□-□), 3 a.u. (◇-◇), 4 a.u. (△-△), 6 a.u. (◁-◁), and 8 a.u. (∇-∇). The laser carrier wavelength $\lambda = 800$ nm.

charge-resonance-enhanced ionization (CREI) [39]. Molecular ions such as H_2^+ have pairs of electronic states [for H_2^+, the $(1\sigma_g, 1\sigma_u)$ states] known as the charge-resonance (CR) state. The CR states will be strongly coupled to the external electromagnetic field at large R, resulting in anomalously high ionization rates. The enhanced ionization rates exceed the atom limit by orders of magnitude, leading to sudden drops of the ratios $W(90°)/W(0°)$. Figure 4 shows the ionization rate of the $1\sigma_g$ state, as functions of the internuclear distance, when the alignment angle $\theta = 0°$. The laser field peak intensity and carrier wavelength are $0.5I_0$ and 800 nm, respectively, for the present calculation. For the reference data [38], comparable parameters of $0.6I_0$ and 790 nm and a different pulse shape are used. Our calculations reproduce the classic two-resonance-peak structure of CREI. Since CREI occurs at

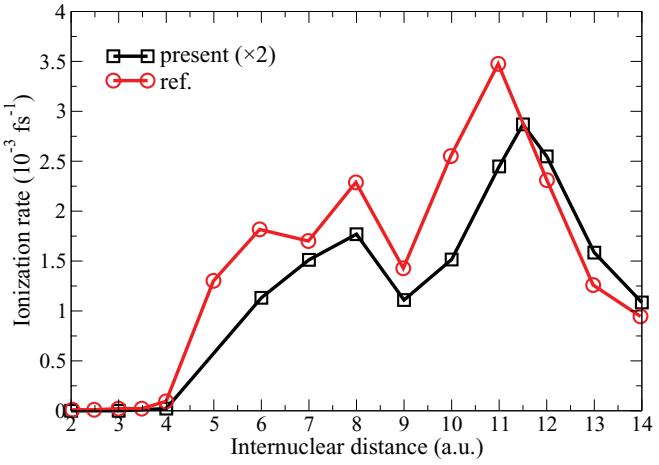

FIG. 4. (Color online) Ionization rate versus internuclear distance for $1\sigma_g$ state of H_2^+, when laser field polarization direction lies parallels to molecular axis ($\theta = 0°$). The laser-field peak intensity and carrier wavelength are $0.5I_0$ and 800 nm, respectively, for the present calculation (□-□,×2), while comparable parameters of $0.6I_0$ and 790 nm are used for the reference data [38](○-○).

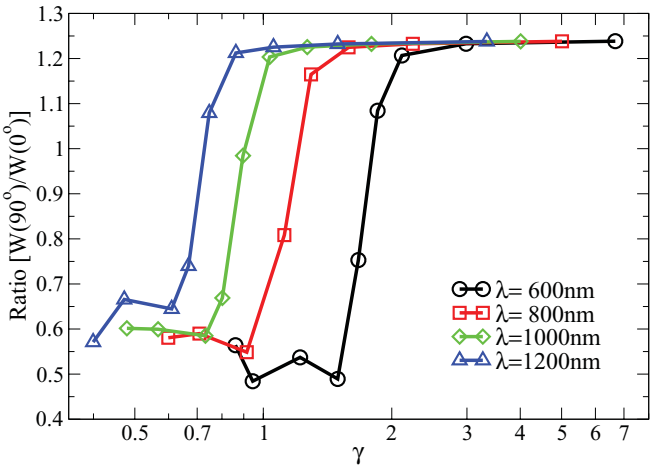

FIG. 5. (Color online) Same as Fig. 3 but for different laser carrier wavelengths: 600 nm (○-○), 800 nm (□-□), 1000 nm (◇-◇), 1200 nm (△-△). The internuclear separation $R = 2$ a.u.

large internuclear distance, we fix R at 2 a.u. to investigate the laser carrier frequency dependence of the transition. In Fig. 5, the ratios of ionization rate $[W(90°)/W(0°)]$ are calculated as functions of the Keldysh parameter, where the laser wavelength takes the values 600, 800, 1000, and 1200 nm, respectively. The transitions take place near the vicinity of $\gamma \approx 1$, although they display a small shift. For $\lambda = 1200$ nm, the ionization enters the tunneling ionization region when $\gamma \leqslant 0.6$. while for $\lambda = 600$ nm, the TI starts to dominate the ionization when $\gamma \leqslant 1.5$. We see that the Keldysh parameter γ works better in the long-wavelength case, in agreement with the tunneling ionization picture. Combining Figs. 3 and 5, the transitions of the ionization ratios can be qualitatively described by the Keldysh parameter γ. The γ-dependent ratio serves as an indicator that can be used to differentiate these ionization channels. In experiments, the internuclear distance can be determined by measuring the ionization ratio in the tunneling region.

B. Comparisons with theoretical models

Next, the TDSE results are compared with those predicted by the strong-field ionization models. In Fig. 6, the ionization rates for the $1\sigma_g$ state are presented as functions of the laser peak intensity, using the TDSE, MO-ADK, LG-SFA, and VG-SFA models. Here the molecule lies parallel to the laser polarization direction. The laser carrier wavelength is 800 nm and the internuclear distance is 2 a.u. In the MPI region ($I < 1.0I_0$), all these models underestimate the TDSE ionization rates. This is no wonder for the MO-ADK model, which is a tunneling model. For the LG-SFA and VG-SFA models, this can be explained by noticing that their single-channel nature, which neglects the intermediate excited states that exist in the full TDSE calculations. In the TI region ($I > 3.0I_0$), the results of the MO-ADK model i agree with results from the TDSE, while the LG-SFA model overestimates and the VG-SFA model underestimates the TDSE results by orders of magnitudes. The strong-field approximation treats the continuum as Volkov states, neglecting the effect of the long-range Coulomb potential with

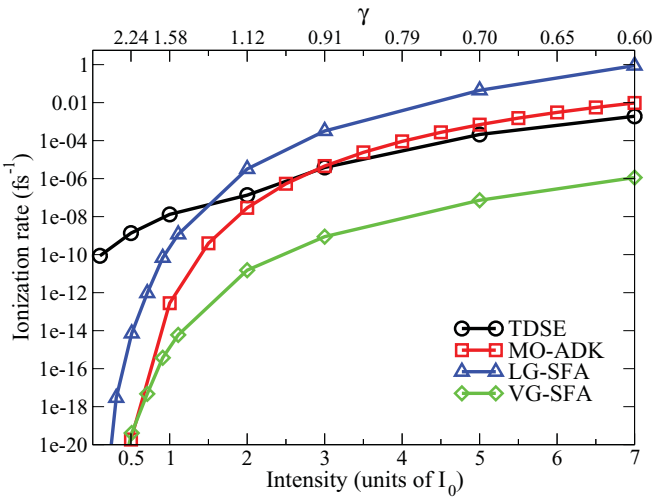

FIG. 6. (Color online) Ionization rate versus laser intensity when $\theta = 0^\circ$ for the $1\sigma_g$ state of H_2^+($R = 2$ a.u.). The rates are calculated from TDSE (○-○), MO-ADK (□-□), LG-SFA (△-△), and VG-SFA (◇-◇), respectively. The corresponding γ value is shown on the upper scale. The laser wavelength is 800 nm.

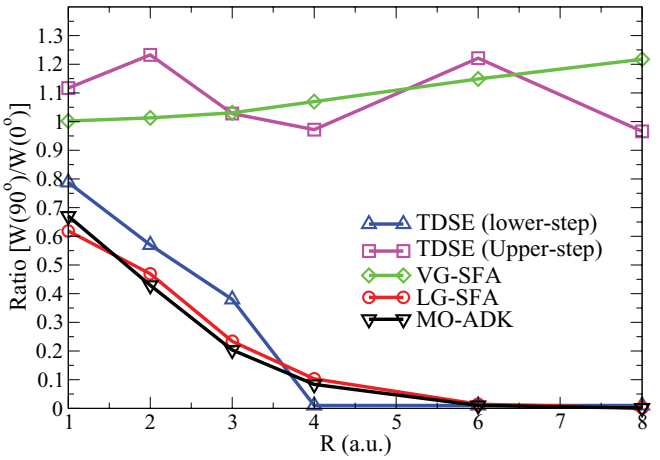

FIG. 8. (Color online) Ratios of ionization rate $[W(90^\circ)/W(0^\circ)]$ versus internuclear distance for the $1\sigma_g$ state of H_2^+. The ratios are calculated from the TDSE (with lower-step △-△, upper-step □-□), VG-SFA(◇-◇), LG-SFA(○-○), and MO-ADK(∇-∇), respectively. For the MO-ADK, LG-SFA, and VG-SFA calculations, the laser intensity $I = 1.0I_0$. The laser wavelength $\lambda = 800$ nm.

the nuclei, which is incorporated in the MO-ADK. In the VG, a correction factor $C_{\mathrm{Coul}} = (\kappa^3/F)^{2Z_c/\kappa}$ was proposed [40] to take into account the Coulomb effects on the final state. SFA models beyond first order are needed to improve the results [41].

We have computed the ratios of ionization rate $[W(90^\circ)/W(0^\circ)]$ for the $1\sigma_g$ state using the TDSE, MO-ADK, LG-SFA, and VG-SFA models, as presented in Fig. 7. Here the laser wavelength is fixed at 800 nm. To avoid the effect of CREI, the internuclear distance of 2 a.u. is used. Unlike the TDSE results, the results predicted by these models display no obvious laser-intensity dependence. In other words, these models fail to predict the transitions between MPI and TI, with the laser intensity varying around the critical position $\gamma \approx 1$. For the MO-ADK model, this is an obvious result because it is a tunneling theory and the approximation is

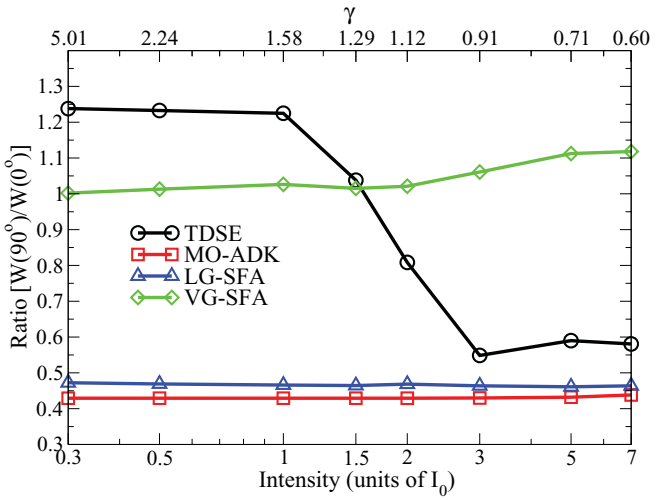

FIG. 7. (Color online) Same as Fig. 6 but for the ratio of ionization rate $[W(90^\circ)/W(0^\circ)]$.

only valid when $\gamma < 1$. The ratios predicted by MO-ADK are 0.43, in qualitatively agreement with ratios predicted by TDSE in the tunneling (lower) step (≈0.58). However, the LG-SFA and VG-SFA models predict qualitatively different ratios. Figure 7 shows that the LG-SFA is applicable in the tunneling region, yielding a ratio of 0.48, which is closer to the TDSE results as compared to MO-ADK. In the multiphoton (higher) step, the VG-SFA yields better results than MO-ADK and LG-SFA. At this region, the VG-SFA predicts the ratio to be ≈1.0, in agreement with the corresponding results of TDSE (1.2).

The ratios presented in Fig. 3 all have two steps. For lager internuclear distances ($R \geqslant 4$ a.u.), although the ratios of the lower steps do not reach their tunneling values due to the affect of CREI, their upper steps can still be referenced. For the sake of clarity, in Fig. 8 we present the ratios on the two steps of the TDSE curves separately, for a wide range of internuclear distances. Note that, for the MO-ADK, LG-SFA and VG-SFA models, the laser intensity is $1.0I_0$, since these ratios are insensitive to the intensity. LG-SFA agrees well with MO-ADK. In fact, LG-SFA recovers the ADK formula in the static-field limit ($\omega \to 0$) [34]. LG-SFA and MO-ADK yield results that agree qualitatively with the results of the TDSE in the tunneling region, while agreement is found between VG-SFA and TDSE in the multiphoton region. A similar disagreement between LG-SFA and VG-SFA was also found in the calculation of strong-field ionization for the highest occupied molecular orbital (HOMO; $3\sigma_g$ state, ionization potential = 15.58 eV) of N_2 in Ref. [13]. For the laser intensity of $1.5I_0$ and a carrier wavelength of 800 nm, the ratios $W(90^\circ)/W(0^\circ)$ predicted by the VG-SFA, LG-SFA, and experiment [19] are 1.25, 0.05, and 0.25, respectively. The Keldysh parameter in this case is approximately 0.9, corresponding to the near-tunneling region. We expect an experiment with a lower laser intensity (larger γ) to verify this.

V. CONCLUSION

In this paper, we have performed *ab initio* calculations of the strong-field ionization from the ground state of H_2^+ by numerically solving the 3D-TDSE. We used prolate spheroidal coordinates and the discrete-variable representation in these coordinates. The ground-state wave functions were obtained accurately by diagonalizing the field-free Hamiltonian. The wave functions were demonstrated to have correct asymptotic behaviors as compared to the GAMESS wave functions and were used to calculate the asymptotic coefficients for MO-ADK and as input wave functions for the calculations of LG-SFA and VG-SFA.

We have found that the ratios of ionization rates computed by TDSE depend critically on the Keldysh parameter γ. As γ varies, the ratios display a two-step structure. For small internuclear distances, the transitions take place around the Keldysh parameter $\gamma \approx 1$ and were considered to be competition between the multiphoton ionization and tunneling ionization. For large distances the transition positions shift to higher values of γ due to charge-resonance-enhanced ionization. The parameter γ works better in the long-wavelength case. Calculations showed that the ratios predicted by MO-ADK, LG-SFA, and VG-SFA displayed no obvious laser-intensity dependence and no such step-like structure. However, LG-SFA and MO-ADK yielded results that qualitatively agreed with TDSE results in the tunneling region, while agreement was found between VG-SFA and TDSE in the multiphoton region. For multielectron systems, the binding energy of the lower orbital may differ from that of the valence electron orbital by several eVs, therefore the ionization of electron from the lower orbital can be hardly considered as tunnel ionization and the total ionization rates might show different alignment dependence based on the observation of the present work. We expect further investigation helps to clarify the discrepancy between experiments and the ADK-like theory on the ionization of more complex molecules.

ACKNOWLEDGMENTS

This work was supported by the National NSF of China under Grants No. 10676039 and No. 10874245, the Major Research plan of National NSF of China (Grant No. 91121017), the National High-Tech ICF Committee of China, and the Innovation Foundation of NUDT under Grant No. B110204.

[1] T. Brabec and F. Krausz, Rev. Mod. Phys. **72**, 545 (2000).
[2] J. H. Posthumus, Rep. Prog. Phys. **67**, 623 (2000).
[3] P. Saliéres, A. L'Huillier, P. Antoine, and M. Lewenstain, Adv. At. Mol. Opt. Phys. **41**, 83 (1999).
[4] F. Krausz and M. Ivanov, Rev. Mod. Phys. **81**, 163 (2009).
[5] M. F. Kling and M. J. J. Vrakking, Annu. Rev. Phys. Chem. **59**, 463 (2008).
[6] M. Protopapas, C. H. Keitel, and P. L. Knight, Rep. Prog. Phys. **60**, 389 (1997).
[7] H. Stapelfeldt and T. Seideman, Rev. Mod. Phys. **75**, 543 (2003).
[8] X. M. Tong, Z. X. Zhao, and C. D. Lin, Phys. Rev. A **66**, 033402 (2002).
[9] T. K. Kjeldsen, C. Z. Bisgaard, L. B. Madsen, and H. Stapelfeldt, Phys. Rev. A **71**, 013418 (2005).
[10] L. V. Keldysh, Zh. Eksp. Teor. Fiz. **47**, 1945 (1964) [Sov. Phys. JETP **20**, 1307 (1965)].
[11] F. H. M. Faisal, J. Phys. B **6**, L89 (1973).
[12] H. R. Reiss, Phys. Rev. A **22**, 1786 (1980).
[13] B. Zhang and Z. X. Zhao, Phys. Rev. A **82**, 035401 (2010).
[14] T. K. Kjeldsen and L. B. Madsen, J. Phys. B **37**, 2033 (2004).
[15] C. Leone, S. Bivona, R. Burlon, F. Morales, and G. Ferrante, Phys. Rev. A **40**, 1828 (1989).
[16] G. L. Kamta and A. D. Bandrauk, Phys. Rev. A **71**, 053407 (2005).
[17] D. A. Telnov and Shih-I Chu, Phys. Rev. A **76**, 043412 (2007).
[18] L. Tao, C. W. McCurdy, and T. N. Rescigno, Phys. Rev. A **79**, 012719 (2009); **80**, 013402 (2009).
[19] D. Pavičić, K. F. Lee, D. M. Rayner, P. B. Corkum, and D. M. Villeneuve, Phys. Rev. Lett. **98**, 243001 (2007).
[20] J. Itatani, D. Zeidler, J. Levesque, M. Spanner, D. M. Villeneuve, and P. B. Corkum, Phys. Rev. Lett. **94**, 123902 (2005).
[21] E. Wells, M. J. DeWitt, and R. R. Jones, Phys. Rev. A **66**, 013409 (2002).
[22] S. Petretti, Y. V. Vanne, A. Saenz, A. Castro, and P. Decleva, Phys. Rev. Lett. **104**, 223001 (2010).
[23] B. K. McFarland, J. P. Farrell, P. H. Bucksbaum, and M. Gühr, Science **322**, 1232 (2008).
[24] O. Smirnova, Y. Mairesse, S. Patchkovskii, N. Dudovich, D. Villeneuve, and P. Corkum, Nature (London) **460**, 08253 (2009).
[25] M. Abramowitz and I. A. S. C. Slater, *Handbook of Mathematical Functions* (Dover, New York, 1965).
[26] L. Malegat, P. Selles, and A. K. Kazansky, Phys. Rev. A **60**, 3667 (1999).
[27] D. A. Telnov and Shih-I Chu, Phys. Rev. A **71**, 013408 (2005).
[28] C. L. Lawson, R. J. Hanson, D. Kincaid, and F. T. Krogh, ACM Trans. Math. Software **5**, 308 (1979); **14**, 1 (1988); **16**, 1 (1990).
[29] E. Anderson, Z. Bai, C. Bischof, S. Blackford, J. Demmel, J. Dongarra, J. Du Croz, A. Green-baum, S. Hammarling, A. McKenney, and D. Sorensen, LAPACK *User's Guide*, 3rd ed. (SIAM, Philadelphia, 1999).
[30] M. M. Madsen and J. M. Peek, At. Data **2**, 171 (1971).
[31] M. V. Ammosov, N. B. Delone, and V. P. Krainov, Zh. Eksp. Teor. Fiz. **91**, 2008 (1986) [Sov. Phys. JETP **64**, 1191 (1986)].
[32] B. Zhang and Z. X. Zhao, Chin. Phys. Lett. **27**, 043301 (2010).
[33] R. N. Zare, *Angular Momentum* (Wiley, New York, 1988).
[34] G. F. Gribakin and M. Y. Kuchiev, Phys. Rev. A **55**, 3760 (1997).
[35] D. Bauer, D. B. Milošević, and W. Becker, Phys. Rev. A **72**, 023415 (2005).
[36] M. W. Schmidt *et al.*, J. Comput. Chem. **14**, 1347 (1993).
[37] T. H. Dunning Jr., J. Chem. Phys. **90**, 1007 (1989); R. A. Kendall, T. H. Dunning Jr., and R. J. Harrison, *ibid.* **96**, 6769 (1992).
[38] L. Y. Peng, D. Dundas, J. F. McCann, K. T. Taylor, and I. D. Williams, J. Phys. B **36**, L295 (2003).
[39] T. Zuo and A. D. Bandrauk, Phys. Rev. A **52**, 2511(R) (1995).
[40] J. Muth-Bohm, A. Becker, and F. H. M. Faisal, Phys. Rev. Lett. **85**, 2280 (2000).
[41] A. Becker and F. H. M. Faisal, J. Phys. B **38**, R01 (2005).